

Phase conjugation of mutually incoherent light beams in a photorefractive medium

A. A. Zozulya and A. V. Mamaev

Institute for Problems in Mechanics, USSR Academy of Sciences

(Submitted 8 June 1989)

Zh. Eksp. Teor. Fiz. 97, 101–113 (January 1990)

We propose a novel phase-conjugation method for two mutually incoherent beams of light, based on coupled ring cavity geometry. A theoretical description of our approach makes it possible to determine the power characteristics, as well as the mode structure of the counterpropagating radiation at the threshold of oscillation. Experimental results are in good agreement with theoretical predictions. We discuss several applications.

1. INTRODUCTION

Phase conjugation of low-power continuous-wave (cw) laser radiation with attendant amplification is a problem with important practical applications. One way to achieve the objective is to configure a mutually-pumped phase conjugation^{1–3} system employing photorefractive crystals. These systems make it possible to conjugate two mutually incoherent laser beams, one weak and the other strong, while at the same time coupling energy from the latter to the former. As a result of the phase conjugation, the weak beam can come away with considerably enhanced intensity relative to its original value. Phase conjugation systems have also been used to phase-lock the radiation from two or more lasers.^{4,5}

In this paper, we describe a novel approach to mutually-pumped phase conjugation in an oscillating configuration (a brief description of which was given in Ref. 6) that differs fundamentally from previous feedback designs. We have carried out the first theoretical analysis for a configuration of this type, incorporating a three-dimensional model for the determination of the mode structure of the scattered radiation near the oscillation threshold, and a nonlinear one-dimensional model for calculating the power characteristics. The proposed configuration has been implemented experimentally. Outstanding features include a low oscillation threshold, no requirements that the beams be carefully focused, and the widest range among existing designs^{1–3} of the intensity ratio between the two beams yielding phase conjugation.

The geometry of the system is as follows (see Fig. 1); two laser beams A_{21} and A_{22} are incident upon the two regions 1 and 2 containing nonlinear photorefractive media (we employ the doubly-subscripted notation A_{ij} for electromagnetic waves, where the first subscript $i = 1–4$ conforms to the standard notation for four-wave mixing, and the second $j = 1–2$ designates the medium in which the interaction takes place). Having traversed one nonlinear medium, each beam is redirected to the other medium by a set of mirrors, and there it interacts with the other beam. For example, after crossing region 1 along path L_1 , beam A_{21} is sent to region 2 (where its designation becomes A_{42}), where it overlaps beam A_{22} . Likewise, after crossing region 2 over path L_2 , beam A_{22} is sent to region 1, where it overlaps beam A_{21} .

In this type of system, absolute instability (oscillation) give rise to scattered radiation counterpropagating with respect to the input beams, with the temporal coherence of the scattered light counterpropagating relative to the signal beam A_{21} being controlled by beam A_{22} , and vice versa. In each of the two regions, wave-vector overlap of the interact-

ing beams creates four holographic index gratings. Since the coherence time of the signal beams A_{21} and A_{22} under typical experimental conditions is much less than the typical response time of the photorefractive medium, only one grating is effectively excited—the one written by coherent pairs of signal and scattered waves. Reading this grating out with the signal beams closes the feedback loops that generate the scattered radiation.

2. THEORETICAL ANALYSIS. GENERAL RELATIONS AND THREE-DIMENSIONAL LINEAR MODEL

We employ a simplified set of coupled equations for our theoretical analysis of four-wave mixing in the beam-overlap regions. If one averages over an interval longer than the coherence time of either of the signal beams A_{21} and A_{22} , this set of equations becomes identical to the set usually employed (e.g., see Ref. 7), which describes four-wave mixing in a photorefractive medium into which a single holographic grating has been written. If the relative transverse displacement of the beams over the path length in each of the interaction regions is small ($\theta l/d \ll 1$, where θ is the angle between the beams, l is the path length in the nonlinear medium, and d is the typical transverse size of the beams), then neglecting diffraction, this set of equations reduces to

$$\begin{aligned} \frac{\partial}{\partial z} A_{1j} &= -v_j A_{4j}, & \frac{\partial}{\partial z} A_{2j} &= -v_j A_{3j}, \\ \frac{\partial}{\partial z} A_{3j} &= v_j A_{2j}, & \frac{\partial}{\partial z} A_{4j} &= v_j A_{1j}, \end{aligned} \quad (1)$$

$$v_j = -\gamma_j (A_{1j} A_{4j}^* + A_{2j} A_{3j}^*) / I_{0j}, \quad I_{0j} = \sum_{i=1}^4 |A_{ij}|^2.$$

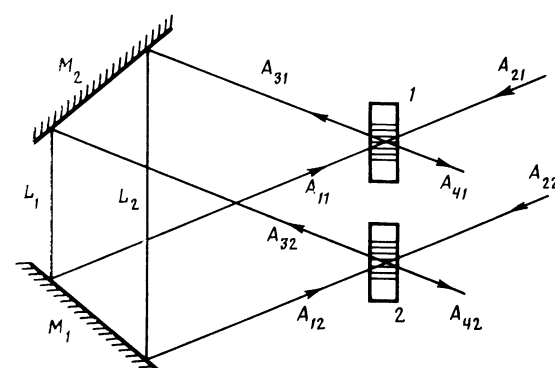


FIG. 1. Geometry for mutually-pumped phase conjugation. Regions 1 and 2 contain photorefractive media, and M_1 and M_2 are beam-bending mirrors.

Here γ_j is the nonlinear coupling coefficient, the nonlinear medium occupies the region $0 < z < l_j$, and derivatives in this system are taken (in the present approximation) along the common direction of propagation z . Transverse to the beam propagation direction, the coordinate $\mathbf{r} = (x, y)$ acts as a parameter in (1). The system (1) is to be supplemented by boundary conditions that specify the incoming signal beams, as well as the free-space diffraction of the signal and scattered radiation in the external optical train formed by the mirrors (Fig. 1):

$$\begin{aligned} A_{21}(\mathbf{r}, l_1) &= a(\mathbf{r}), \quad A_{22}(\mathbf{r}, l_2) = b(\mathbf{r}), \\ A_{31}(\mathbf{r}, l_1) &= A_{32}(\mathbf{r}, l_2) = 0, \\ A_{42}(\mathbf{r}, 0) &= \hat{L}_1 A_{21}, \quad A_{41}(\mathbf{r}, 0) = \hat{L}_2 A_{22}, \\ A_{11}(\mathbf{r}, 0) &= \hat{L}_1 A_{32}, \quad A_{12}(\mathbf{r}, 0) = \hat{L}_2 A_{31}. \end{aligned} \quad (2)$$

Here \hat{L}_j is the diffraction operator, with

$$\begin{aligned} \hat{L}_j A &= \frac{T^{1/2} k_0}{2\pi i L_j} \exp(i\varphi_j) \int dx' dy' A(x', y', 0) \\ &\times \exp\left\{\frac{ik_0}{2L_j} [(x+x')^2 + (y-y')^2]\right\}. \end{aligned} \quad (3)$$

T in Eq. (3) is the (intensity) reflection coefficient of the mirror system, φ_j is the phase shift over path L_j , k_0 is the wave vector of the radiation, x is measured in the plane of incidence of the signal beams, y is perpendicular to it, and the two-mirror geometry shown in Fig. 1 rotates (inverts) the image about the x axis.

Under typical experimental conditions, the optical path length L is some tens of centimeters, and the transverse beam dimension d is typically of the order of several millimeters. The Fresnel number $N = k_0 d^2 / L$ will then be much greater than unity, and variations in the spatial structure of the beams propagating through the optical train will be associated with their nonvanishing wavefront curvature. Writing the electromagnetic fields at the boundary of the nonlinear medium in the form

$$A_{ij}(\mathbf{r}, 0) = B_{ij}(\mathbf{r}, 0) \exp[ik_0 r^2 / 2R_{ij}], \quad (4)$$

where B_{ij} specifies the transverse structure of the beam, and varies slowly compared to an exponential, while R_{ij} is the beam's radius of curvature, we obtain from Eqs. (2) and (3) the following behavior for the radii of curvature of the signal beams as they propagate along the external optical train:

$$\begin{aligned} R_{42}^{-1} &= L_1^{-1} (1 - \alpha_1^{-1}), \quad R_{41}^{-1} = L_2^{-1} (1 - \alpha_2^{-1}), \\ \alpha_j &= 1 + L_j / R_{2j} \quad (j = 1, 2). \end{aligned} \quad (5)$$

Similarly, for the scattered radiation we obtain

$$\begin{aligned} R_{1j}^{-1} &= L_j^{-1} (1 - \beta_j^{-1}), \\ \beta_1 &= 1 + L_1 / R_{32}, \quad \beta_2 = 1 + L_2 / R_{31}. \end{aligned} \quad (6)$$

For the functions B_{ij} , the boundary conditions (2) and (3) yield

$$\begin{aligned} B_{42}(x, y, 0) &= T^{1/2} \alpha_1^{-1} \exp(i\varphi_1) B_{21}(-x/\alpha_1, y/\alpha_1, 0), \\ B_{41}(x, y, 0) &= T^{1/2} \alpha_2^{-1} \exp(i\varphi_2) B_{22}(-x/\alpha_2, y/\alpha_2, 0), \\ B_{11}(x, y, 0) &= T^{1/2} \beta_1^{-1} \exp(i\varphi_2) B_{32}(-x/\beta_1, y/\beta_1, 0), \\ B_{12}(x, y, 0) &= T^{1/2} \beta_2^{-1} \exp(i\varphi_1) B_{31}(-x/\beta_2, y/\beta_2, 0). \end{aligned} \quad (7)$$

It is clear from (7) that α_j and β_j are essentially transverse scaling coefficients for the cross sections of the beams as they propagate through the external optical train.

The conditions for cancellation of rapid phase variations associated with the radii of curvature of the beams in each of the interaction regions yield the system of equations $R_{ij}^{-1} + R_{2j}^{-1} - R_{3j}^{-1} - R_{4j}^{-1} = 0$ ($j = 1, 2$), which has two solutions:

$$\beta_1 = \alpha_1^{-1}, \quad \beta_2 = \alpha_2^{-1}, \quad (8a)$$

$$\beta_1 = \alpha_2 (\alpha_1 \alpha_2 L_1 + L_2) (\alpha_1 \alpha_2 L_2 + L_1)^{-1}, \quad \beta_2 = \alpha_1 \alpha_2 \beta_1^{-1}. \quad (8b)$$

The solution (8a) corresponds to the situation in which the phase component associated with the wavefront curvature of the scattered beams is conjugate to the corresponding component of the signal beams:

$$R_{3j} = -R_{4j}, \quad R_{1j} = -R_{2j}. \quad (9)$$

The second solution does not possess this property. To determine the conditions under which the present configuration phase-conjugates the signal beams, we shall analyze the solution (8a), and ascertain just when it is feasible. Mathematically, the boundary-value problem formulated here consists of the two sets of equations (1) for each of the interaction regions plus the boundary conditions (7) and (8a). The solution of (1) is well known,⁸ which makes it possible to reduce the boundary problem to a set of algebraic and transcendental nonlocal equations interrelating the values of B_{ij} ($z = 0$) at different values of the transverse coordinate r .

A similar approach has been used in a three-dimensional analysis of the nonlinear characteristics of a stimulated-Brillouin-scattering (SBS) ring cavity.⁹ A full solution of the nonlinear problem is rather involved, and must be obtained numerically. We therefore restrict ourselves here to the region near threshold, which enables us to determine the mode structure of the scattered radiation for the present configuration, as well as the threshold for mode excitation. A threshold analysis relies on the amplitude of the scattered radiation being small compared with that of the signal beams: $A_{1j}, A_{3j} \ll A_{2j}, A_{4j}$. Assuming the signal beam amplitudes A_{2j} and A_{4j} to be given, and introducing the form factors for the scattered radiation

$$F_{1j}(\mathbf{r}, z) = A_{1j}(\mathbf{r}, z) / A_{2j}(\mathbf{r}), \quad F_{3j}(\mathbf{r}, z) = A_{3j}(\mathbf{r}, z) / A_{4j}(\mathbf{r}), \quad (10)$$

we may use the boundary conditions $F_{3j}(\mathbf{r}, l_j) = 0$ from (1) to obtain

$$F_{3j}(\mathbf{r}, 0) = F_{1j}(\mathbf{r}, 0) P_j(\mathbf{r}), \quad (11)$$

$$P_j(\mathbf{r}) = \exp\left(\gamma_j l_j \frac{1-D_j}{1+D_j}\right) \left[1 - D_j \exp\left(\gamma_j l_j \frac{1-D_j}{1+D_j}\right)\right]^{-1},$$

where $D_j = |A_{4j}(\mathbf{r})/A_{2j}(\mathbf{r})|^2$.

The form factors for the scattered radiation leaving the system are then

$$F_{1j}(\mathbf{r}, l_j) = F_{3j}(\mathbf{r}, 0) (1 - D_j) \left[\exp\left(\gamma_j l_j \frac{1-D_j}{1+D_j}\right) - 1\right]^{-1}. \quad (12)$$

Boundary conditions (7), (8a), and (11) yield the system of equations

$$\begin{aligned} F_{31}(x, y, 0) &= T \exp[i(\varphi_2 - \varphi_1)] P_1(\mathbf{r}) F_{32}(-\alpha_1 x, \alpha_1 y, 0), \\ F_{32}(x, y, 0) &= T \exp[i(\varphi_1 - \varphi_2)] P_2(\mathbf{r}) F_{31}(-\alpha_2 x, \alpha_2 y, 0), \end{aligned} \quad (13)$$

whose solution, along with (12), provides complete information on the transverse structure of the scattered beams.

This set of equations can be put into formal correspondence with the usual linear unstable resonator (see Ref. 10, Chapter 3), the theory of which implies that solutions of (13) will be stable when

$$|\alpha_1\alpha_2| < 1. \quad (14)$$

Solutions of (13), inasmuch as they are modes of the nonlinear oscillator under consideration, form an infinite series, and can be labeled with three indices m, n, l the first two defining the transverse structure of a mode, and the last being associated with the frequency shift of the scattered radiation relative to the frequency of the signal beams. This shift enters into Eq. (13) through the nonlinear coupling coefficients γ_j , which in general are complex quantities that depend on the frequency difference between the electromagnetic waves that write an index grating into the nonlinear medium; they also depend on the external electromagnetic field occasionally imposed on the crystal to control the magnitude of the real and imaginary parts of the coefficient γ .¹¹ If the latter field is not present (as we shall assume from here on), then $\gamma_j = \gamma_j^{(0)}(1 - i\Delta\tau_j)^{-1}$ where $\gamma_j^{(0)}$ is real, $\Delta = \omega_1 - \omega_2$ is the frequency difference between the scattered and signal radiation, and τ_j is the relaxation time of the medium.

An analysis of Eqs. (13) shows that the frequency-shifted modes have comparatively high excitation thresholds. In particular, the most interesting modes from a practical standpoint are those in the $(m, n, 0)$ family, which have zero frequency shift (i.e., $l = 1$) and therefore yield real coupling coefficients γ_j . Near the coordinate origin ($r \rightarrow 0$), the transverse structure of an (m, n) mode (omitting the third index, which equals 0) has the asymptotic form $F^{(m,n)}(x, y) \sim x^m y^n$ (m and n are nonnegative integers). The threshold for an (m, n) mode as $r \rightarrow 0$ follows from (13), and is given by

$$1 = T^2(\alpha_1\alpha_2)^{m+n} P_1(0)P_2(0), \quad (15)$$

which determines the threshold dependence of the nonlinear coupling constants γ_1, γ_2 for excitation of an (m, n) mode on the transmission coefficient T of the optical train, on the ratio $\rho = |A_{22}(0)/A_{21}(0)|^2$ of the intensities as the centers of the signal beams incident upon the first and second interaction regions, and on the scaling factors α_1, α_2 for the signal-beam cross sections as they pass through the optical train. Hereafter, to avoid further complication, we examine the case of identical nonlinear coupling constants $\gamma_1 l_1 = \gamma_2 l_2 = \gamma l$.

We see then from (15) that the mode structure of the present device is independent of the phase difference between φ_1 and φ_2 accumulated during propagation of the two beams along different paths in the optical train; in other words, it is insensitive to the path lengths L_1, L_2 . This remains true as long as the path-length difference $|L_1 - L_2|$ is less than the coherence length of both of the incident beams.

An analysis of the dependence of the mode-generation thresholds on the coefficients α_1, α_2 shows that the mode-stability condition (14) also selects modes according to their excitation threshold, with the minimum threshold belonging to the $(0, 0)$ mode. The mode-excitation thresholds increase

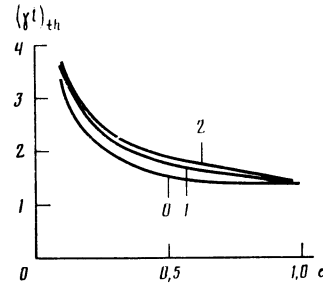


FIG. 2. Threshold value of the nonlinearity coefficient $(\gamma l)_{th}$ as a function of the scaling coefficient α of the incident beams, for $\rho = 1$ and $T = 0.33$. The curves are labeled by the value of $m + n$.

with decreasing α_j . For example, with $\alpha_1 = \alpha_2 = \alpha$ and $\rho = 1$, Eq. (15) yields for the threshold value of the coupling coefficient γl

$$(\gamma l)_{th} = \frac{\alpha^2 + T}{\alpha^2 - T} \ln \frac{\alpha^2(1 + T|\alpha|^{m+n})}{T(1 + |\alpha|^{m+n+2})}. \quad (16)$$

In Fig. 2 we have plotted the α -dependence of $(\gamma l)_{th}$ for a few of the lowest-order modes with low-lying excitation thresholds.

It is worth noting that the mode indices m and n , which define the mode structure relative to the x and y axes, respectively, enter into (15) and (16) as a sum; that is, the x and y axes are on an equal footing. This results from neglecting the noncollinearity of the overlapping beams in our model (the thin-medium model). In Ref. 12, which dealt with the mode structure of an SBS ring oscillator in the opposite case of a medium that completely fills the entire beam-overlap region, it was demonstrated that noncollinearity of the beams provides for selection of the radiation in the plane of intersection (x axis), so that beam compression is only required for selection with respect to the y axis, i.e., the x and y coordinates are no longer on an equal footing.

An analysis of the dependence of mode-generation thresholds on the intensity ratio ρ of the signal beams shows that the threshold increases at both high and low values of ρ , attaining a minimum at some intermediate value, which depends on the scaling factors α_1 and α_2 . In other words, for some given value of the nonlinearity constant γl , oscillation takes place over a finite range of values of the parameter ρ . As $\rho \rightarrow \infty$, the threshold for mode (m, n) given by (15) be-

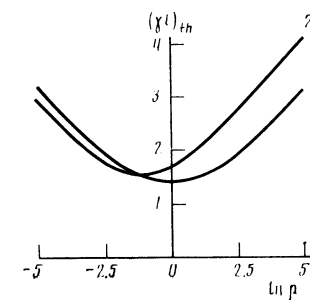


FIG. 3. Threshold value of the nonlinearity coefficient $(\gamma l)_{th}$ for generating the lowest mode as a function of the intensity ratio ρ for the centers of the signal beams. Curve 1: $\alpha_1 = \alpha_2 = 0.8$, $T = 0.33$; curve 2: $\alpha_1 = 0.9$, $\alpha_2 = 0.3$, $T = 0.33$.

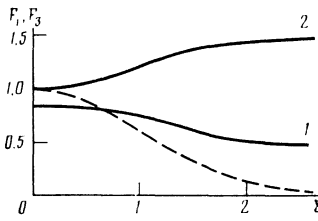


FIG. 4. Form factors for scattered radiation at the system output (F_1 , curve 1) and within the optical train (F_3 , curve 2) for incident beams with the Gaussian intensity distribution $|A_{21}(\mathbf{r})| = |A_{22}(\mathbf{r})| = \exp(-\xi^2/2)$, for $\alpha_1 = \alpha_2 = 0.8$, $T = 0.33$. The dashed curve is $\exp(-\xi^2/2)$.

comes

$$\exp[-2(\gamma l)_{th}] = \rho^{-1} T \alpha_2^2 (\alpha_1 \alpha_2)^{m+n}. \quad (17)$$

For $\rho \rightarrow 0$, (15) yields

$$\exp[-2(\gamma l)_{th}] = \rho \alpha_1^2 T (\alpha_1 \alpha_2)^{m+n}. \quad (18)$$

In Fig. 3, we have plotted the ρ -dependence of the oscillation threshold $(\gamma l)_{th}$ for both equal and unequal values of the scaling factors α_j , for the lowest available threshold of the (0,0) excitation mode.

Using Eqs. (12) and (13), a knowledge of the threshold values $(\gamma l)_{th}$ enables one to determine the spatial structure of any mode at its excitation threshold, having specified as input the spatial distributions of the signal waves $A_{21}(\mathbf{r})$ and $A_{22}(\mathbf{r})$. Figure 4 shows plots of the scattered-radiation form factors within the optical train ($F_{3j}(\mathbf{r}, 0)$) and at the system output ($F_{1j}(\mathbf{r}, l)$) for identical signal beams with a Gaussian intensity distribution

$$|A_{21}(\mathbf{r})|^2 = |A_{22}(\mathbf{r})|^2 = \exp[-(x^2 + y^2)/d^2] = \exp(-\xi^2),$$

where d is the beam diameter, all for equals scaling factors $\alpha_1 = \alpha_2 = 0.8$ for the (0,0) mode. The vertical axis shows the value of $F_3(\xi) = F_{31}(\mathbf{r}, 0) = F_{32}(\mathbf{r}, 0)$ and $F_1(\xi) = F_{11}(\mathbf{r}, l) = F_{12}(\mathbf{r}, l)$, and the horizontal axis shows the value of ξ . Perfect phase conjugation would correspond to coordinate-independent form factors F_1 and F_3 ; departures from a constant value characterize the extent to which accurate phase conjugation takes place. Note that when γl is real, so are the functions F_1 and F_3 , so that the phase structure of the scattered radiation, according to (9), is completely reversed, and the amplitude structure is distorted. This situation arises only when γl is real. For complex values of the coupling constant, corresponding either to frequency shifts of the scattered radiation or to the presence of an electrostatic field in the crystal, the phase structure of the scattered beams would also be distorted.

3. ONE DIMENSIONAL NONLINEAR MODEL

The most systematic way to ascertain the power characteristics of the present design is to make use of a three-dimensional nonlinear model. The most satisfactory description of system behavior above threshold, however, is provided by a one-dimensional nonlinear model, the principal advantage of which is its simplicity. In the one-dimensional approach, the transverse structure of the interacting beams is not taken into account by (1), which describes four-wave mixing in each of the interaction regions; the boundary conditions (2)

and (3) are replaced by

$$A_{21}(l) = a, \quad A_{22}(l) = b, \quad A_{31}(l) = A_{32}(l) = 0, \quad (19)$$

$$A_{42}(0) = T^{1/2} \exp(i\varphi_1) A_{21}(0), \quad A_{41}(0) = T^{1/2} \exp(i\varphi_2) A_{22}(0), \\ A_{12}(0) = T^{1/2} \exp(i\varphi_2) A_{31}(0), \quad A_{11}(0) = T^{1/2} \exp(i\varphi_1) A_{32}(0),$$

Introducing the nonlinear reflection coefficients

$$R_1 = |A_{11}(l)/a|^2, \quad R_2 = |A_{12}(l)/b|^2 \quad (20)$$

for the signal waves and determining the dimensionless parameter $\rho = |b/a|^2$, which equals the ratio of signal-wave intensities fed to the first and second interaction regions, we find that the boundary conditions (19) and the integrals of the motion of the system (1) yield

$$R_1/R_2 = \rho^2, \quad (21)$$

while to determine the absolute value of $R_{1,2}$, we obtain from the solution to the boundary-value problem (1), (19)

$$\frac{G_{11}G_{21}}{G_{31}G_{41}} = \frac{G_{12}G_{22}}{G_{32}G_{42}}, \quad (22)$$

where

$$G_{1j} = 1 - \exp \mu_j, \\ G_{2j} = (\Delta_j + 2d_j - Q_j) + (\Delta_j + 2d_j + Q_j) \exp \mu_j, \\ G_{3j} = (\Delta_j - Q_j) - (\Delta_j + Q_j) \exp \mu_j, \\ G_{4j} = d_{2j}(\Delta_j - Q_j + 2R_j d_{2j}) - d_{2j}(\Delta_j + Q_j + 2R_j Q_j) \exp \mu_j. \quad (23)$$

In (23), we have used the notation $\Delta_j = d_{1j} - d_{2j}$, $Q_j = (\Delta_j^2 + 4R_j d_{2j}^2)^{1/2}$, $\mu_j = -\gamma_j l_j Q_j (d_{1j} + d_{2j})^{-1}$, $d_{11} = T\rho$, $d_{12} = T$, $d_{21} = 1$, $d_{22} = \rho$.

Equation (22) has infinitely many solutions, corresponding to different frequency offsets of the scattered radiation relative to the signal-wave frequency—that is, to different longitudinal modes, in the language of the previous three-dimensional analysis. In the present context, there are no transverse modes. The lowest-lying mode has zero frequency shift, corresponding to purely real values of the coupling coefficient γ_j . From here on we shall examine only that mode. Its excitation threshold may be obtained by letting R_1 , $R_2 \rightarrow 0$ in (22) and (23); in the simplest case, with $\rho = 1$, we have

$$(\gamma l)_{th} = \frac{1+T}{1-T} \ln \frac{1+T}{2T}. \quad (24)$$

Comparison of (24) with (16) shows that the threshold behavior as a function of the transmission coefficient of the optical train as given by the one-dimensional model is qualitatively correct, but that the two equations will be identical only when $\alpha = 1$, in which case the present design provides no selectivity among transverse modes.

The oscillation threshold increases when ρ becomes either greater than or less than unity. For large enough values of the coupling coefficient γl , the range of signal-wave intensity ratios for which oscillation takes place is given by

$$T^{-1} \exp(-2\gamma l) < \rho < T \exp(2\gamma l), \quad (25)$$

which is approximately the same as obtained from the three-dimensional considerations leading to (17) and (18) with $\alpha_{1,2} \approx 1$.

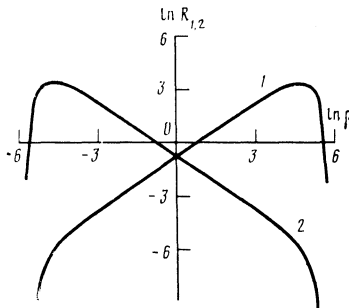


FIG. 5. Incident-beam nonlinear reflection coefficients R_1 (curve 1) and R_2 (curve 2) as functions of beam intensity ratio ρ for $T = 0.5$, $\gamma l = 3$.

An increase in the nonlinear coupling coefficient relative to its threshold value leads to an increase in the nonlinear reflection coefficients R_1 and R_2 . The maximum possible value of the reflection coefficients, resulting from large values of the nonlinear coupling coefficient, correspond to a complete conversion of the energy in each signal beam into radiation conjugate to the other beam, allowing for the transmission coefficient of the optical train:

$$R_{1\max} = T\rho, \quad R_{2\max} = T/\rho. \quad (26)$$

Figure 5 shows the typical behavior of the nonlinear reflection coefficients R_1 and R_2 as a function of ρ ; these curves were obtained from (21)–(23) with $T = 0.5$, $\gamma l = 3$. The reflection coefficients are the same for $\rho = 1$, and are almost equal to the maximum attainable value $R = T$ (26). Equation (26) provides a good description of the behavior of $R_{1,2}(\rho)$ in Fig. 5 for $\rho \neq 1$ as well, but not for values of ρ that are too large or too small. Further increases or decreases in ρ at fixed γl bring the system back down toward threshold, and reduce the reflection coefficients. The maximum signal-wave intensity ratio for which oscillation takes place, for the parameters used in Fig. 5, is $\rho_{\max} \approx 200$, and the maximum value of the reflection coefficient for the weaker beam is $R \approx 27$.

4. THE EXPERIMENT

The experimental setup is shown in Fig. 6. The two mutually incoherent beams were derived from 2-mW LG-52-1 and LG-52-2 helium-neon lasers ($\lambda = 0.63 \mu\text{m}$), and were steered to nonlinear medium C_1 by the rotary mirrors M_1 and M_2 . The nonlinear medium was cerium-doped barium-strontium niobate (SBN)¹³ approximately 3 mm thick. The two beams, propagating approximately parallel to one another, were ≈ 2 mm in diameter inside the crystal, and were separated by ≈ 6 mm. Both the optical axis of the crystal and the plane of polarization of the laser beam lay in the plane of incidence.

After passing through crystal C_1 , the beams were re-

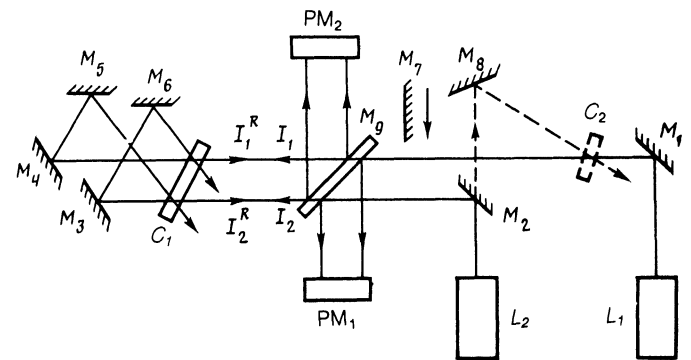


FIG. 6. Experimental setup. L_1 , L_2 : helium-neon lasers; M_1 – M_8 : beam-steering mirrors; M_9 : half-silvered beam-splitter with $R \approx 10\%$; C_1 , C_2 : photorefractive crystals of SBN:Ce; PM_1 , PM_2 : power meters.

directed by mirrors M_3 – M_6 back through the crystal at an angle of 40° in such a way that each beam overlapped the other. The optical path lengths L_1 and L_2 (see Fig. 1) were about 40 cm, and with due allowance for absorption in the crystal, losses due to Fresnel reflection at the crystal facets, and mirror losses, the (intensity) transmission coefficient T was approximately 33%.

The beam splitter M_9 , located in front of C_1 , enabled us to monitor both the incident power (I_1 , I_2) and the return power (I_1^R , I_2^R) using power meters PM_1 and PM_2 , respectively. The incident power was varied using half-wave plates and polarizers (not shown in Fig. 6). The nonlinear interaction in the crystal resulted in the appearance of phase-conjugate radiation appearing after ~ 100 sec. The spatial structure of this radiation depended on the ratio of the diameters d_1 and d_2 of the first and second laser beams on their first pass through C_1 , to their diameters d'_1 and d'_2 afterwards. These ratios could be adjusted using positive and negative lenses in the feedback loop.

In Fig. 7 we have reproduced photographs of the counterpropagating radiation for three different values of beam compression. In Fig. 7a, we have $\alpha_1 d'_1/d_1 \approx 1.8$, $\alpha_2 d'_2/d_2 \approx 1$; for Fig. 7b, $\alpha_1 \approx 1.8$, $\alpha_2 \approx 0.7$; for Fig. 7c, $\alpha_1 \approx 1.8$, $\alpha_2 \approx 0.45$. Theoretically, violation of the condition $|\alpha_1 \alpha_2| < 1$ results in substantially greater divergence of the counterpropagating radiation than of the incident beams. This increase occurs only along the y axis, however, perpendicular to the overlap plane of the beams; it thus has no bearing upon our model, in which the x and y coordinates are on an equal footing. The reason is that the thin-medium approximation assumed in the theory is not entirely consistent with the experiment, and a correct treatment would require that one take account of the noncollinearity of the beams in the overlap region. As $|\alpha_1 \alpha_2|$ approaches unity, the beam divergence along the y axis decreases (Fig. 7b), and for $|\alpha_1 \alpha_2| < 1$ (Fig. 7c), the counterpropagating radiation has a

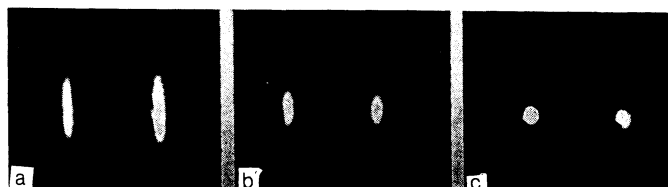


FIG. 7. Photographs of the intensity distribution of the phase-conjugate radiation. a) $\alpha_1 \approx 1.8$, $\alpha_2 \approx 1$; b) $\alpha_1 \approx 1.8$, $\alpha_2 \approx 0.7$; c) $\alpha_1 \approx 1.8$, $\alpha_2 \approx 0.45$.

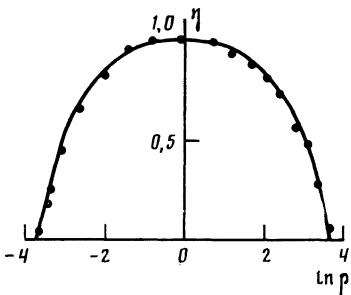


FIG. 8. Experimental points and theoretical dependence of the normalized sum of counterpropagation intensities $\eta = (I_1^R + I_2^R)/(I_1^R + I_2^R)_{\max}$ as a function of the incident-beam intensity ratio $\rho = I_2/I_1$ for $I_1 + I_2 = \text{const.}$

divergence comparable to that of the incident beams.

To test for the presence of a phase-conjugate wavefront, a glass “phase” plate of nonuniform thickness was placed in the beam path in front of crystal C_1 , and focusing lenses were placed in the feedback loop to collect the light scattered past the phase plate and to provide beam-compression factors $\alpha_{1,2}$ close to unity. The fraction of phase-conjugate light in the counterpropagating beams, as measured using a standard method,¹⁴ was $\sim 80\%$.

In this experiment, we also studied the effect of the optical path difference $|L_1 - L_2|$ on the oscillation process; this difference was adjusted by moving mirrors M_3 , M_6 and M_4 , M_5 . We found that as long as the difference $|L_1 - L_2|$ is much less than the coherence length of either laser, it has no influence on oscillation. Upon further increase in the difference $|L_1 - L_2|$, the intensity of the counterpropagating radiation falls off, and when $|L_1 - L_2| \approx 40$ cm (which in the present case is comparable to the laser coherence length), generation ceases.

The power characteristics of this design were measured for incident-beam values of α_1 and α_2 close to unity. In Fig. 8, we have plotted experimental values of the normalized sum of counterpropagating intensities $\eta = (I_1^R + I_2^R)/(I_1^R + I_2^R)_{\max}$ for $I_1 + I_2 = \text{const}$ as function of $\rho = I_2/I_1$ (I_1 and I_2 are the incident beam intensities). The overall reflection coefficient $R = (I_1^R + I_2^R)/(I_1 + I_2)$ for the entire optical train is maximized at $\rho = 1$, and allowing for Fresnel reflection at the input facet of the crystal, it comes to approximately 25%. Note also that the experimental points in Fig. 8 are symmetrically disposed about the vertical axis. If the optics were to become misaligned and the beams overlapped less in one region than in the other, the peak of the curve would be displaced to the left or right.

We compared the theoretical data in Fig. 8 with theory in the following manner. Equating Eqs. (22) and (23) with the experimental value of the maximum intensity ratio $\rho_{\max} \approx 40$ for which oscillation ceases, we found the value of the nonlinear coupling constant γl . Having assumed an overall transmission coefficient $T = 33\%$, we obtained $\gamma l \approx 2.3$. We then constructed the curve for $\eta(\rho)$ shown in Fig. 8, making use of Eqs. (22) and (23) with $\gamma l \approx 2.3$ and $T = 33\%$. The theoretical value of the maximum reflection coefficient R is approximately 28%, in good agreement with the experimental data. We also checked the theoretical relation (21) experimentally; the measured points showing I_1^R/I_2^R as a function of $\rho = I_2/I_1$ and the corresponding

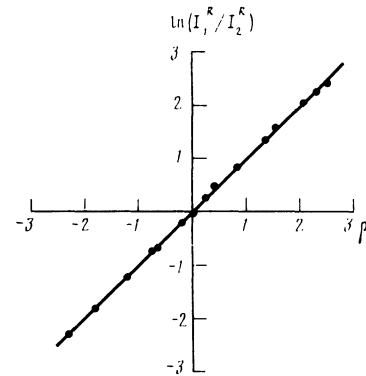


FIG. 9. Ratio of counterpropagating intensities I_1^R/I_2^R as a function of the incident-beam intensity ratio $\rho = I_2/I_1$. Experimental results are shown as points; the straight line is given by theory.

theoretical straight line are plotted in Fig. 9.

Notice that with unequal incident beam intensities, it is simple to obtain a reflection coefficient greater than unity for the weaker beam. This has enabled us to observe oscillation in a cavity comprised of a plane mirror and a phase-conjugating mirror. Theory predicts, however, that such a cavity will only operate under “hard” excitation conditions—that is, it requires a very specific level of seed radiation. In our experiment, we therefore made two beams of approximately equal intensity overlap in crystal C_1 (Fig. 6), and then after the appearance of counterpropagating radiation, one of the beams was blocked and mirror M_7 was positioned in the optical path and oriented normal to the incident beam. The intensity ratio between the phase-conjugate radiation and the pump radiation incident on crystal C_1 and provided by beam I_2 was about 6%. The theoretical value obtained by solving the one-dimensional system (1) with appropriately modified boundary conditions is approximately 7%, in good agreement with the experimental results.

We also point out that a phase conjugation system enables one to attack the problem of receiving and returning a weak signal with gain. In fact, since the beam conjugate to the signal beam has the frequency of the second laser, that same laser can be used to simplify the radiation returned by using a dynamic hologram. This arrangement has been implemented experimentally. To do so (see Fig. 6), mirror M_2 was replaced by a semitransparent beam splitter with reflection coefficient $\sim 10\%$. The radiation passing through that splitter (indicated by a dashed line) was reversed by mirror M_8 and sent on to crystal C_2 (SBN:Ce), which was similar to C_1 . Two-wave mixing in C_2 then produced amplification of the phase-conjugate radiation I_1^R . The overall reflection coefficient obtained experimentally for the incident radiation I_1 was approximately 20.

5. CONCLUSIONS

In discussing this experiment, we have compared theoretical models designed to describe the present configuration with experimental data. We will now also compare this configuration with others that have appeared previously.¹⁻⁴ As we do so, it should be borne in mind that there has been no detailed theoretical analysis for Refs. 1–3 to compare theory with experiment quantitatively. The theoretical models proposed in Refs. 1 and 15 treat scattering in these systems as a

consequence of the development of oscillation (absolute instability). But for the configuration discussed in Ref. 1, for example, a three-dimensional analysis similar to the one carried out in Ref. 12 shows that this setup is not an oscillator, and that scattering is due to convective instability. The applicability of the models advanced in Refs. 1 and 15 to the actual experimental situation is a problem that requires close study. Subsequent comparisons must be undertaken with this in mind.

In comparing the theoretical models, the configuration of Ref. 1 has the lowest threshold among those discussed in Refs. 1–4 (γl)_{th,min} = +2. At the same time, within the context of the one-dimensional model, the configuration that we have examined here has a threshold only half as high. Again, among the configurations in Refs. 1–4, the range of signal-beam intensity ratios ρ at which phase conjugation takes place is the widest in the setup of Ref. 1, where it is given approximately by $\exp(-\gamma l) < \rho < \exp(\gamma l)$. For our device, we estimate a much wider range: $T^{-1} \exp(-2\gamma l) < \rho < T \exp(2\gamma l)$.

There are no experimental data on the range of beam intensity ratios ρ for the configuration of Ref. 1; for those of Refs. 2 and 3, $0.1 < \rho < 2$ and $0.5 < \rho < 5$, respectively. Furthermore, for the latter system, both reflection coefficients are low over the entire range of ρ ($\lesssim 25\%$). With the crystals that we used in the configuration proposed here, $1/40 < \rho < 40$.

In the present paper, thus we have proposed a novel configuration for phase conjugation of mutually incoherent light beams in a photorefractive medium. We have carried

out a theoretical analysis of this system, including the construction of a three-dimensional linear model for determining the mode structure of the scattered radiation at the threshold of oscillation, and a one-dimensional nonlinear model for calculating its power characteristics. The proposed configuration has been realized experimentally, and the empirical results have been compared with theory.

- ¹S. Weiss, S. Sternklar, and B. Fischer, Opt. Lett. **12**, 114 (1987).
- ²A. M. C. Smout and R. W. Eason, Opt. Lett. **12**, 498 (1987).
- ³M. D. Ewbank, Opt. Lett. **13**, 47 (1988).
- ⁴S. Sternklar, S. Weiss, M. Segev, and B. Fischer, Opt. Lett. **11**, 528 (1986).
- ⁵M. Segev, S. Weiss, and B. Fischer, Appl. Phys. Lett. **50**, 1397 (1987).
- ⁶A. A. Zozulya and A. V. Mamaev, Pis'ma Zh. Eksp. Teor. Fiz. **49**, 483 (1989) [JETP Lett. **49**, 553 (1989)].
- ⁷M. Cronin-Golomb, B. Fischer, J. O. White, and A. Yariv, IEEE J. Quantum Electron. **20**, 12 (1984).
- ⁸A. A. Zozulya and V. T. Tikhonchuk, Kvant. Elektron. (Moscow) **15**, 1570 (1988) [Sov. J. Quantum Electron. **18**, 981 (1988)].
- ⁹V. V. Eliseev, A. A. Zozulya, and V. T. Tikhonchuk, Fiz. Inst. AN SSSR, Preprint No. 22 (1989).
- ¹⁰Yu. A. Znan'ev *Optical Cavities and the Problem of Laser Beam Divergence* [in Russian], Nauka, Moscow (1979).
- ¹¹N. V. Kikhtarev, V. B. Markov, S. G. Odulov, M. S. Soskin, and V. L. Vinetskii, Ferroelectrics **22**, 949 (1979).
- ¹²A. A. Zozulya, V. P. Silin, and V. T. Tikhonchuk, Zh. Eksp. Teor. Fiz. **92**, 788 (1987) [Sov. Phys. JETP **65**, 443 (1987)].
- ¹³I. R. Dorosh, Yu. S. Kuzminov, N. M. Polozkov, et al., Phys. Status Solidi A **65**, 513 (1981).
- ¹⁴B. Ya. Zel'dovich, N. F. Pilipetskii, and V. V. Shkunov, *Phase Conjugation* [in Russian], Nauka, Moscow (1985).
- ¹⁵Qi-che He, IEEE J. Quantum Electron. **24**, 2507 (1988).

Translated by Marc Damashek